Cluster folding optical potential analysis for ^{6}Li + ^{28}Si elastic scattering

Sh. Hamada[a] and Awad A. Ibraheem[b,c]

[a]*Faculty of Science, Tanta University, Tanta, Egypt.*
[b]*Physics Department, King Khalid University, Abha, Saudi Arabia.*
[c]*Physics Department, Al-Azhar University, Assiut Branch, Assiut 71524, Egypt.*
e-mail: sh.m.hamada@science.tanta.edu.eg, awad_ah_eb@hotmail.com

Received 14 September 2020; accepted 17 November 2020

Available experimental angular distributions for ^{6}Li + ^{28}Si elastic scattering in the energy range 16-318 MeV are reanalyzed phenomenologically based on an optical model using Woods-Saxon (WS) potentials for both real and imaginary parts as well as semi microscopically based on cluster folding potential. The generated cluster folding potential is based on the appreciable cluster structure and breakup of ^{6}Li into a deuteron orbiting a core of α-particle. Although several data sets in a wide range of energies are subjected to investigation, the theoretical calculations using the different concerned potentials reproduce fairly well the experimental data in the whole energy range. The extracted real and imaginary volume integrals and reaction cross-sections values are compared to the previously reported ones, and they are found to be in good agreement.

Keywords: Elastic scattering; phenomenological potential; cluster folding; coupled channels.

PACS: 21.10.Jx; 21.60.Cs; 24.10.Eq; 25.70.Hi

DOI: https://doi.org/10.31349/RevMexFis.67.276

1. Introduction

The study of nuclear processes induced by weakly bound nuclei such as ^{6}Li, ^{7}Li, ^{10}Be, ^{11}Be, has attracted plenary attention for years. Especially, the processes induced by ^{6}Li and ^{7}Li nuclei gained attention due to the break-up effect of ^{6}Li into $d + \alpha$, and ^{7}Li into $t + \alpha$ which plays a crucial role in the elastic scattering of ^{6}Li and ^{7}Li, for a range of target nuclei at different energies. There are extensive experimental measurements and theoretical studies for ^{6}Li + ^{28}Si nuclear system, and the available data are classified into two categories: experimental data near the Coulomb barrier energy EC [1-7] and the data above EC [8-14]. It is appropriate here to disregard particular effects due to coupling to other reaction channels when studying the elastic scattering mechanisms between two ions at energies well above the EC. In this case, the elastic scattering data can be reproduced well by utilizing the conventional optical and folding potentials. On the other hand, at energies near the EC, the coupling effects are significant and appear in various reaction channels. Pakou *et al*. [1] measured the angular distributions for ^{6}Li + ^{28}Si at four near barrier energies -7.5, 9, 11, and 13 MeV - over a wide angular range. The data were analyzed using optical potential with the real part derived based on double folding (DF) potential. It was found that the strength of the real part of potential remains almost independent of the energy, and in order to reproduce the data, a reduction in the renormalization factor by about 40% is necessary. Sinha *et al*. [5] measured the angular distributions for ^{6}Li + ^{28}Si at energies 16 and 21 MeV. The measured data, as well as the data at lower energies, were fitted using optical potentials of both imaginary volume and surface parts. The effect of the break-up on elastic scattering was investigated within the Continuum Discretized Coupled Channels (CDCC) method. Experimental data at high energies [10-14] showed refractive features at forwarding angles region, in contrast to the data at low energies close to EC. Nadasen *et al*. [14] measured the angular distribution for ^{6}Li + ^{28}Si at 318 MeV; the data extend well beyond the rainbow angle into the region where the far-side scattering dominates. The data were reproduced reasonably well using DF potential without renormalization. The data at high energies [8-14] were also subjected to various optical model (OM) and DF analysis. The ^{6}Li + ^{28}Si system has been subjected to several theoretical studies [15-21] recently, which were devoted to investigating this nuclear system either at low and high energies using different pure OM and DF potentials. M. Anwar [17] analyzed the experimental angular distributions of ^{6}Li scattered elastically by different targets $-^{24}$Mg, ^{28}Si, ^{40}Ca, ^{48}Ca, ^{58}Ni, ^{90}Zr, and ^{11}6Sn - at E_{lab} (^{6}Li) = 240 MeV. The data were analyzed using the conventional OM potential as well as DF of two different effective density independent nucleon-nucleon *NN* interactions namely S1Y and M3Y. The analysis incorporated four different forms of ^{6}Li density distribution with rms radii ranging from 2.195 to 2.444 fm. The DF analysis, for the concerned data, showed that the strength of the real part of potential should be reduced by a factor of $\approx$ 28% - 0.36%. M. A. Hassanain *et al*. [19] investigated the ^{6}Li + ^{28}Si elastic scattering at six energy sets ranging from 76 to 318 MeV, using two approaches. In the first approach, the full α cluster structure of the interacting nuclei was considered, where ^{6}Li was described in terms of $d-\alpha$ cluster model wave function, and the ^{28}Si nucleus was described as 7α. In the second approach, the real part of the potential was constructed based

on the CDM3Y6 Paris *NN* interaction. They reported that the quality of fitting directly proportional to the energy, as expected, and a renormalization factor of $\approx 0.43 - 1.0$ is required to fit the data.

Yongli Xu *et al.* [21] performed a systematic global optical model description for ^{6}Li projectiles scattered elastically from targets ranging from ^{24}Mg to ^{209}Bi at energies below 250 MeV. The obtained global optical potential from this study was found to be applicable for different elastic scattering processes induced by ^{6}Li. The obtained potential is also used to predict the reaction cross sections for targets outside the concerned mass range.

Y. Sakuragi [22] studied the projectile break-up effects on the elastic scattering of ^{6}Li from different targets with a mass number ($A = 12 - 208$). The ^{6}Li break-up effects were investigated, within the framework of the CDCC method, in the elastic scattering cross-sections with interaction potentials extracted from the M3Y DF potential. The calculations could reproduce the experimental elastic scattering data for all the studied targets and incident energies without any renormalization for the folded potential if an additional term "Dynamic Polarization Potential DPP" was introduced. The DPP has a repulsive real part with a strength of $\approx 40\%$ of the folding potential. For nucleons, $\alpha-$particles and heavy ions ($A_P \geq 10$), at energies up to 20 MeV/nucleon, the folding potential is successful in fitting the experimental data with $N_R \approx 1.0$. However, the optical potential for ^{6,7}Li [22-26], based on a folding model, has been found unsuccessful since the values of N_R required in order to fit the data are much smaller than unity. Theoretical studies for ^{6}Li-target systems present a problem in the DF model description, where the real potential requires a renormalization of approximately one-half in order to reproduce the data. Branden *et al.* [27] assumed that this is due to the importance of break-up channels for the loosely bound ^{6}Li nucleus, represented by a complex DPP, which has a strongly repulsive real part. It is to be noted that several theoretical calculations [22,28,29], including CDCC calculations, showed that the renormalization factor is close to unity when the coupling to break-up channels is included.

The available experimental measurements for ^{6}Li + ^{28}Si system at high energies and over sufficiently wide angular range reveal several ambiguities associated with the different concerned potentials. In the present work, the ^{6}Li + ^{28}Si nuclear system is subjected to further investigation. Firstly, a new systematic global description for the data is obtained using the conventional OM potential of fixed radii parameters. Secondly, motivated by the well-known cluster nature of ^{6}Li, the data are reanalyzed from the microscopic point of view in the cluster folding optical model (CFOM) framework. The ^{6}Li + ^{28}Si angular distributions data are plotted as a function of momentum transfer, and they showed that the same real part of potential could be used to reproduce the data at different energies as they exhibit the same oscillatory behavior in the forward angle region. Finally, the concerned data are well described using non-renormalized real cluster folding potential when an additional dynamical polarization term is added.

The paper is organized as follows. In Sec. 2, the theoretical calculations for ^{6}Li + ^{28}Si system based on both optical and cluster folding potentials are described. Section 3 is devoted to the discussion of the results and the summary is given in Sec. 4.

2. Theoretical calculations

Using the phenomenological OM potential and semi microscopically using CFOM potential, the elastic scattering angular distributions for ^{6}Li + ^{28}Si nuclear system in the energy range $16 - 318$ MeV are reanalyzed in order to obtain the global potential, which could reproduce the data in this wide range of concerned energies.

2.1. Data analysis within the framework of OM

The elastic scattering angular distributions for ^{6}Li + ^{28}Si nuclear system at energies 16 MeV [5], 20 MeV [6], 21 MeV [5], 25 MeV [7], 27 MeV [8], 32 MeV [9], 34 MeV [8], 99 MeV [10], 135.1 MeV [11], 210 MeV [12], 240 MeV [13], and 318 MeV [14] are investigated within the framework of OM. The parameters considered by A. Nadasen *et al.* [12] are taken as starting parameters. The analyses employed Coulomb potential as well as real and imaginary volume central potentials. As the influence of spin-orbit interaction for ^{6}Li is small, it has been excluded. The used potential is represented in the following form:

$$U(r) = V_C(R) - V f(r, r_x, a_x) - iW f(r, r_x, a_x). \quad (1)$$

Here $f(r, r_x, a_x)$, $x = V$, W is the Woods-Saxon (WS) form factor $(1 + \exp[r - r_x A^{1/3})/a_x])^{-1}$ and $V_C(R)$ is the Coulomb potential due to a uniform sphere with a charge equal to that of the target nucleus and radius $r_C A_t^{1/3}$. The calculations are performed using the code FRESCO [30], and SFRESCO search code is used in searching the optimal potential parameters. Two parameters were fixed during the search r_V, and r_W at values 1.299 fm, and 1.703 fm respectively, and the rest four parameters V_0, a_V, W_0, and a_W are allowed to be changed freely till reach the least χ^2 value, defined by

$$\chi^2 = \frac{1}{N} \sum_{i=1}^{N} \left(\frac{\sigma(\theta_i)^{\text{cal}} - \sigma(\theta_i)^{\text{exp}}}{\Delta\sigma(\theta_i)} \right)^2, \quad (2)$$

where N is the number of experimental data points. $\sigma(\theta_i)^{\text{cal}}$ and $\sigma(\theta_i)^{\text{exp}}$ are the calculated and experimental cross-sections, while $\Delta\sigma(\theta_i)$ is the relative uncertainty in experimental data.

2.2. Data analysis within the framework of CFOM

Considering the appreciable cluster probability of ^{6}Li as a weakly bound $\alpha + d$ system, we try to describe the ^{6}Li elastically scattered from ^{28}Si nucleus using a simple CFOM. In

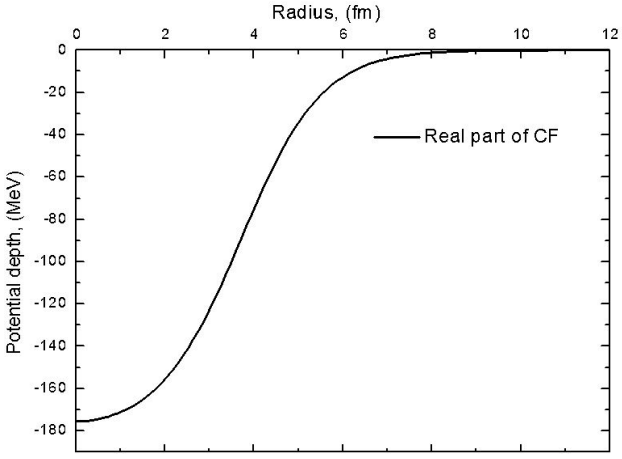

FIGURE 1. Real cluster folding potential used in the present study.

this model, the real part of ^{6}Li + ^{28}Si potential is generated based on cluster folding. For the well-known optical potential of $\alpha-$particles and deuterons, we define the ^{6}Li potential as:

$$V^{CF}(R) = \int \left(V_{\alpha-^{28}\mathrm{Si}} \left[\mathbf{R} - \frac{1}{3}\mathbf{r} \right] + V_{d-^{28}\mathrm{Si}} \left[\mathbf{R} + \frac{2}{3}\mathbf{r} \right] \right) |\chi_{\alpha d}(\mathbf{r})|^2 d\mathbf{r}, \quad (3)$$

where $\chi_{\alpha d}(\mathbf{r})$ is the intercluster wave function for the relative motion of α and d in the ground state of ^{6}Li, and $\mathbf{r}$ is the relative coordinate between the centers of mass of α and d. $V_{\alpha-^{28}\mathrm{Si}}$ and $V_{d-^{28}\mathrm{Si}}$ are the phenomenological potentials for $\alpha + {}^{28}$Si and $d + {}^{28}$Si channels which fairly reproduce the experimental data at the appropriate energies $E_d \approx 1/3E_{Li}$ and $E_\alpha \approx 2/3E_{Li}$ taken from [31,32]. $\alpha - d$ bound state form factor represents a 2*S* state in a real WS potential with $V_0 = 79.0$ MeV, $R = 1.15$ fm, $a = 0.7$ fm [33]. The main parameters required to prepare the cluster folding potential for ^{6}Li + ^{28}Si are the optimal potentials for $d + {}^{28}$Si and $\alpha + {}^{28}$Si at appropriate energies. The highest energy under consideration is 318 MeV, so the required potentials are $V_{d+^{28}\mathrm{Si}}$ at $E_{lab} = 1/3 \times 318 = 106$ MeV and $V_{\alpha+^{28}\mathrm{Si}}$ at $E_{lab} = 2/3 \times 318 = 212$ MeV. Unfortunately, there are no experimental measurements at the aforementioned energies. For the second maximum available data for ^{6}Li + ^{28}Si (240 MeV), the required potentials are $V_{d+^{28}\mathrm{Si}}$ at $E_{lab} = 80$ MeV and $V_{\alpha+^{28}\mathrm{Si}}$ at $E_{lab} = 160$ MeV. By searching the previous experimental studies for $d + {}^{28}$Si and $\alpha + {}^{28}$Si nuclear systems, it is found that the most suitable potentials, which could be used to generate the cluster folding potential for ^{6}Li + ^{28}Si are $d + {}^{28}$Si at $E_{\mathrm{lab}} = 52$ MeV [31] and $\alpha + {}^{28}$Si at $E_{lab} = 166$ MeV [32]. The obtained real part for the generated cluster folding potential is presented in Fig. 1.

3. Results and discussion

The comparison between the experimental ^{6}Li + ^{28}Si elastic scattering angular distributions at $E_{lab} = 16 - 318$ MeV and the theoretical calculations based on Woods-Saxon optical potential are shown in Figs. 2-4 and the extracted potential parameters are listed in Table I. The agreement between the experimental data and calculations is fairly good not only at all the concerned energies but also over the entire angular range. The χ^2/N values obtained from this work are comparable to previously reported values [5-14]. Although the radius parameter for both the real and imaginary potential parts are fixed during the search process for potential parameters, no clear dependence of real and imaginary potential depths on energy is obtained.

TABLE I. Global optical potential parameters for ^{6}Li + ^{28}Si nuclear system extracted from the OM analysis, the values of reaction cross sections σ_R as well as real J_V and imaginary J_W volume integrals are also listed.

E (MeV)	V_0 (MeV)	r_V (fm)	a_V (fm)	W_0 (MeV)	r_W (fm)	a_W (fm)	χ^2/N	σ_R (mb)	J_V (MeV.fm^3)	J_W (MeV.fm^3)
16	189.9	1.299	0.684	34.9	1.703	0.941	0.29	1419	376.87	159.67
20	101.75	1.299	0.829	26.65	1.703	0.701	3.2	1177	223.65	108.86
21	189.9	1.299	0.732	45.0	1.703	0.794	1.13	1470	389.42	191.27
25	186.05	1.299	0.754	37.28	1.703	0.737	3.01	1445	387.44	154.32
27	140.63	1.299	0.812	15.78	1.703	0.938	19.9	1560	305.29	72.08
32	189.9	1.299	0.77	34.9	1.703	0.827	11.7	1693	399.96	150.72
34	130.9	1.299	0.926	20.39	1.703	0.922	27.3	1690	309.47	92.37
99	139.17	1.299	0.731	31.51	1.703	0.86	2.5	1783	285.19	138.31
135.1	109.8	1.299	0.87	30.53	1.703	0.95	5.4	1905	248.81	140.33
210	129.9	1.299	0.84	33.52	1.703	0.782	3.97	1609	287.85	141.67
240	117.01	1.299	0.841	29.17	1.703	0.891	2.3	1687	259.48	130.05
318	115.3	1.299	0.86	30.32	1.703	0.783	3.9	1502	259.32	128.20

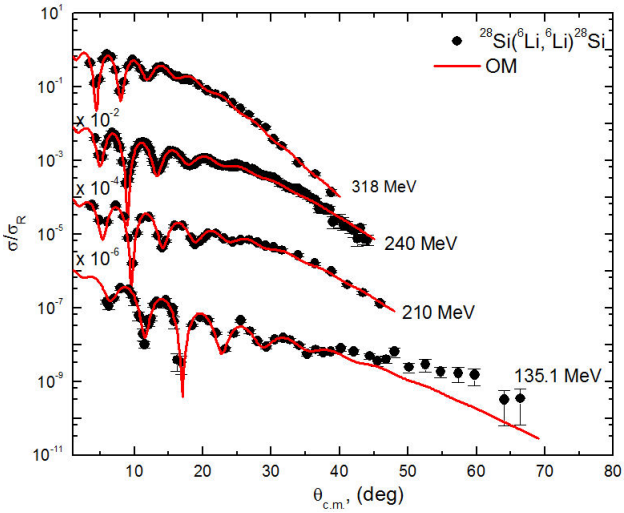

FIGURE 2. Comparison between experimental angular distributions data (solid black circles) and theoretical calculations for ^{28}Si(^{6}Li,^{6}Li)^{28}Si elastic scattering at E_{lab} = 318, 240, 210, and 135.1 MeV. The solid red curves denote OM fits.

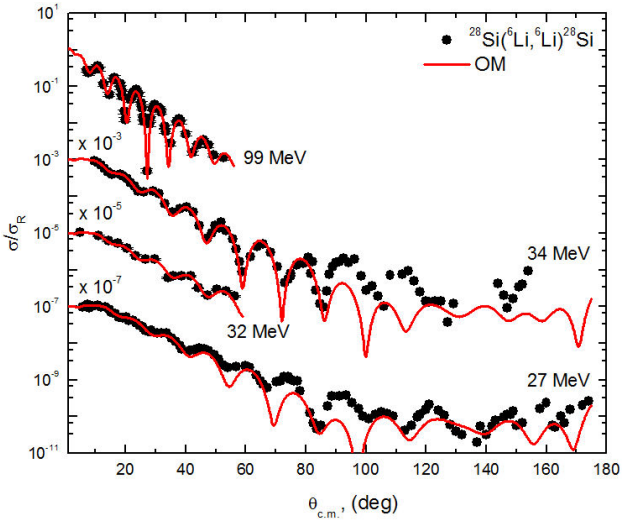

FIGURE 3. Same as Fig. 2 but at E_{lab} = 99, 34, 32, and 27 MeV.

In CFOM, the theoretical calculations are performed using a real part of the potential derived based on mentioned cluster folding "see Eq. (3)" in addition to an imaginary Woods-Saxon term. Thus, the nuclear potential takes the following shape:

$$U(R) = V_C(R) - N_{RCF}V^{CF}(R) - iW(R). \qquad (4)$$

The comparison between the experimental angular distributions for ^{6}Li + ^{28}Si elastic scattering and the theoretical calculations performed within the framework of CFOM are shown in Figs. 5-7, while the potential parameters are listed in Table II. The same potential parameters for the imaginary volume term, extracted from the OM analysis, are kept the same in CFOM calculations. Consequently, the data are fitted using only one parameter- N_{RCF}, "which is the renormalization factor for the real part of potential derived based on

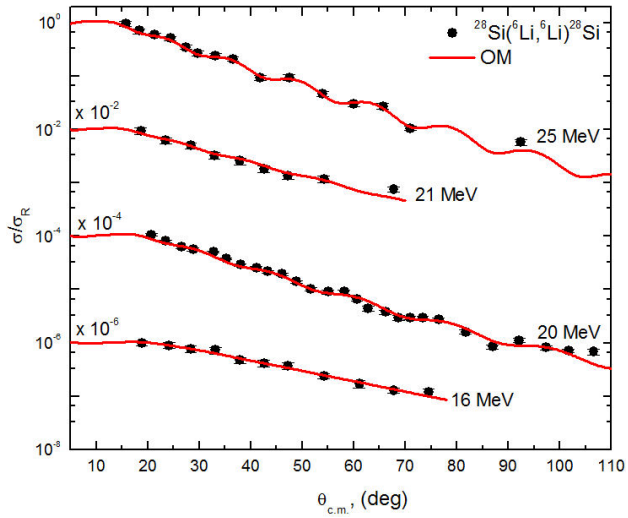

FIGURE 4. Same as Fig. 2 but at E_{lab} = 25, 21, 20, and 16 MeV.

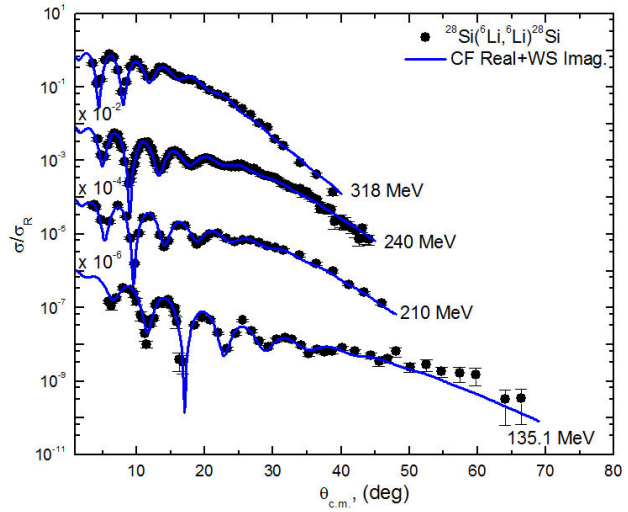

FIGURE 5. Comparison between experimental angular distributions data (solid black circles) for ^{28}Si(^{6}Li,^{6}Li)^{28}Si elastic scattering and the theoretical calculations (solid blue curves) using CFP plus an imaginary WS potential at E_{lab} = 318, 240, 210, and 135.1 MeV.

cluster folding". As shown in Figs. 5-7, the agreement between the experimental data and the calculations is good, and the χ^2/N values are close to those obtained from OM analysis or even better at some energies. The extracted average value for N_{RCF} is 0.732 ± 0.1, indicating that the strength of N_{RCF} should be reduced by about 27% in order to reproduce the data. The same problem was reported previously in DF analysis for ^{6}Li + X nuclear systems, where X is a different target nucleus such as ^{12}C, ^{16}O, ^{28}Si.

The elastic scattering angular distributions for the ^{6}Li + ^{28}Si nuclear system at the different concerned energies are plotted as a function of momentum transfer as shown in Fig. 8. The data at relatively higher energies displayed a complex oscillatory behavior with periodic structures of different periods at forwarding angles. The interference peaks and valleys line up, whereas if they are plotted as a function of

TABLE II. Potential parameters for ^{6}Li + ^{28}Si nuclear system extracted from the CFOM analysis, the values of reaction cross sections σ_R as well as real J_V and imaginary J_W volume integrals are also listed.

E (MeV)	N_{RCF}	W_0 (MeV)	r_W (fm)	a_W (fm)	χ^2/N	σ_R (mb)	J_V (MeV.fm^3)	J_W (MeV.fm^3)
16	0.5 ± 0.01	34.9	1.703	0.941	0.58	1432	177.77	159.67
20	0.598 ± 0.01	26.65	1.703	0.701	3.2	1175	212.61	108.86
21	0.814 ± 0.01	45.0	1.703	0.794	2.47	1497	289.42	191.27
25	0.814 ± 0.01	37.28	1.703	0.737	6.2	1459	289.42	154.32
27	0.814 ± 0.01	15.78	1.703	0.938	26.4	1567	289.42	72.08
32	0.753 ± 0.01	34.9	1.703	0.827	15.9	1684	267.73	150.72
34	0.794 ± 0.01	20.39	1.703	0.922	30.1	1690	282.31	92.37
99	0.65 ± 0.01	31.51	1.703	0.86	6.1	1791	231.11	138.31
135.1	0.739 ± 0.01	30.53	1.703	0.95	6.7	1903	262.75	140.33
210	0.83 ± 0.01	33.52	1.703	0.782	4.16	1610	295.11	141.67
240	0.747 ± 0.01	29.17	1.703	0.891	1.99	1687	265.60	130.05
318	0.733 ± 0.01	30.32	1.703	0.783	4.6	1501	260.62	128.20

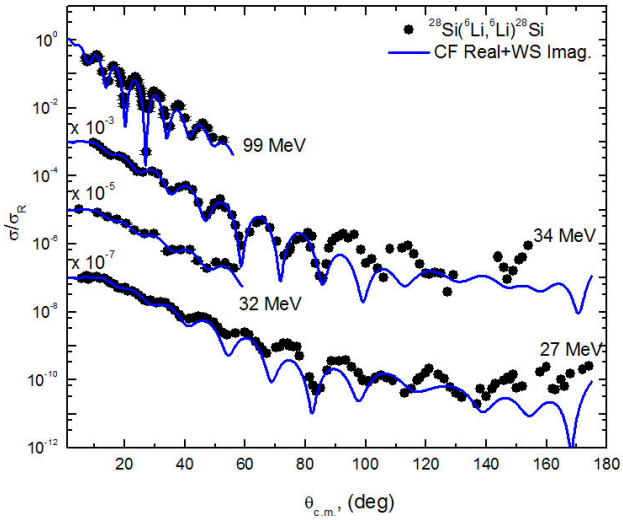

FIGURE 6. Same as Fig. 5 but at $E_{\rm lab} = 99$, 34, 32, and 27 MeV.

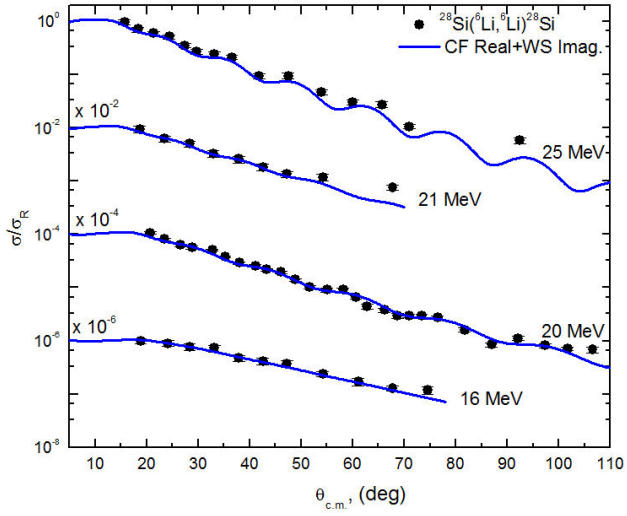

FIGURE 7. Same as Fig. 5 but at $E_{\rm lab} = 25$, 21, 20, and 16 MeV.

angle, there is not an apparent pattern. The formula $q = 2k\sin(\theta_{c.m}/2)$ is used to calculate the cross-sections as a function of momentum, where k is the wavenumber. The wavenumber was taken to be $k = 0.219[Mt/(M_t + M_p)]\mathrm{x}\sqrt{M_p \times E_{lab}}$. Here M_p and M_t are the masses of the projectile and target, respectively. As shown in Fig. 8, the plotted data, as a function of momentum transfer, exhibit dips form at momentum transfers around $q = 0.59$, 1.05, and 1.58 fm^{-1} that can be followed down to an energy of 34 MeV. Consequently, it should be shown that the forward angle dips are produced by the same "potential"; and the differences between the cross-sections at different energies at larger momentum transfer (angles) are due to the absorption at larger values. This is also the reason why the data at lower energies (below 16 MeV) are excluded from this study. The extracted values of N_{RCF} from the CFOM at the different concerned energies are close to each other except for the data for the data at lower energies, which showed some deviations as shown in Table II. Therefore, if N_{RCF} is adjusted to 0.732 -the average extracted value from CFOM analysis- and is allowed for a slight variation for W_0 and a_W, the data could be reproduced with the same real cluster folding potential.

The strong absorption at relatively high energies leads to refractive features such as the nuclear rainbow followed by structure-less falloff, as shown in Fig. 8. The possibility of seeing such refractive features was first realized in the scattering of alpha particles [34]. A few years later, hints emerged that similar but weaker effects were seen in the scattering of light heavy-ions ^{6}Li [11,35] and ^{12}C [36,37]. By now, many examples of refractive phenomena in light heavy-ion systems have been collected already.

TABLE III. Potential parameters for ^{6}Li + ^{28}Si system at different energies using non-renormalized real CFP "$N_{RCF} = 1.0$" plus DPP "surface potential with a repulsive real part" in addition to an imaginary WS potential, r_W is fixed to 1.703 fm.

E (MeV)	N_{RCF}	W_0 (MeV)	r_W (fm)	a_W (fm)	χ^2/N	$V_{\rm pol}$	$r_{\rm pol}$	$a_{\rm pol}$
16	1.0	34.9	1.703	0.941	0.8	-30.14	1.0	0.89
20	1.0	26.65	1.703	0.701	3.3	-30.19	1.0	0.89
21	1.0	45.0	1.703	0.794	2.8	-20.51	1.0	0.805
25	1.0	37.28	1.703	0.737	4.3	-20.49	1.0	0.89
27	1.0	15.78	1.703	0.938	23.8	-20.79	1.0	0.8
32	1.0	34.9	1.703	0.827	16.6	-29.79	1.0	0.82
34	1.0	20.39	1.703	0.922	30.5	-29.79	1.0	0.82
99	1.0	31.51	1.703	0.86	4.7	-23.88	1.1	0.9
135.1	1.0	30.53	1.703	0.95	6.5	-23.72	1.1	0.806
210	1.0	33.52	1.703	0.782	4.2	-17.68	1.0	0.882
240	1.0	29.17	1.703	0.891	1.7	-27.98	1.0	0.839
318	1.0	30.32	1.703	0.783	5.2	-29.31	1.0	0.823

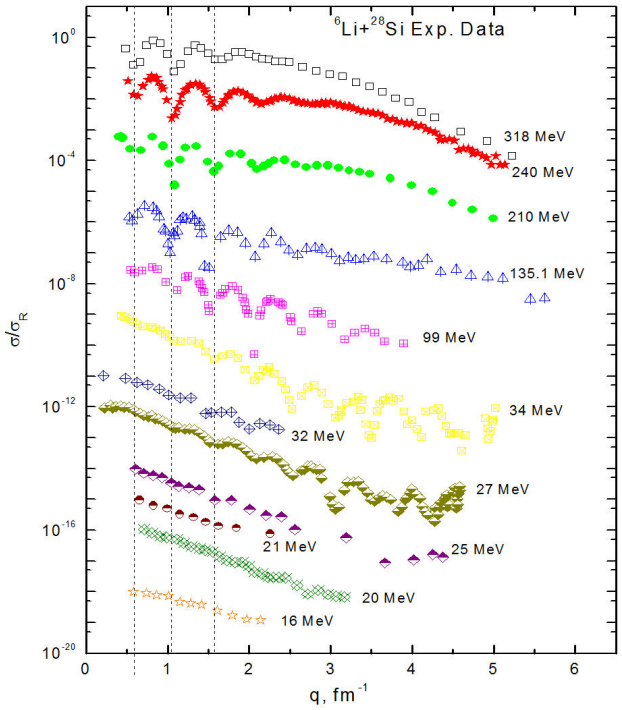

FIGURE 8. Experimental angular distributions for ^{6}Li + ^{28}Si elastic scattering at energies $E_{lab} = 16 - 318$ MeV plotted as a function of momentum transfer.

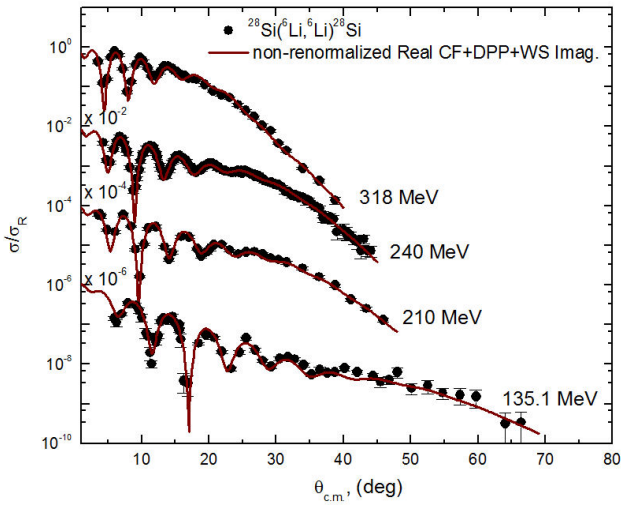

FIGURE 9. Comparison between experimental angular distributions data (solid black circles) for ^{28}Si(^{6}Li,^{6}Li)^{28}Si elastic scattering and the theoretical calculations (solid brown curves) using non-renormalized real CFP plus a DPP term in addition to an imaginary WS potential at $E_{lab} = 318$, 240, 210, and 135.1 MeV.

Previously microscopic analysis for the ^{6}Li + ^{28}Si system presented a problem in the DF, where the real part of potential required a renormalization of approximately one-half in order to reproduce the data, and it was assumed that this is due to the importance of break-up channels for the loosely bound ^{6}Li nucleus. The analysis of ^{6}Li + ^{28}Si scattering data using real CFP in the current work also showed the same trend, as N_{RCF} should be reduced by about 27% in order to reproduce the data. The cluster folding calculations are repeated using non-renormalized real CFP "$N_{RCF} = 1$" with the same, previously obtained imaginary WS potential plus a dynamical polarization potential (surface potential with a repulsive real part designed to simulate the polarization effects caused by the projectile break-up). The used DPP is characterized by three parameters ($V_{\rm pol}$, $r_{\rm pol}$, $a_{\rm pol}$), and their corresponding values at the different concerned energies are listed in Table III. The comparisons between the experimental data and theoretical calculation performed using the non-renormalized real CFP plus the dynamical polarization potential are shown in Figs. 9-11, and they show the same good agreement as in Figs. 5-7.

The best-fitting OM and CFOM parameters, with the corresponding calculated real and imaginary volume integrals

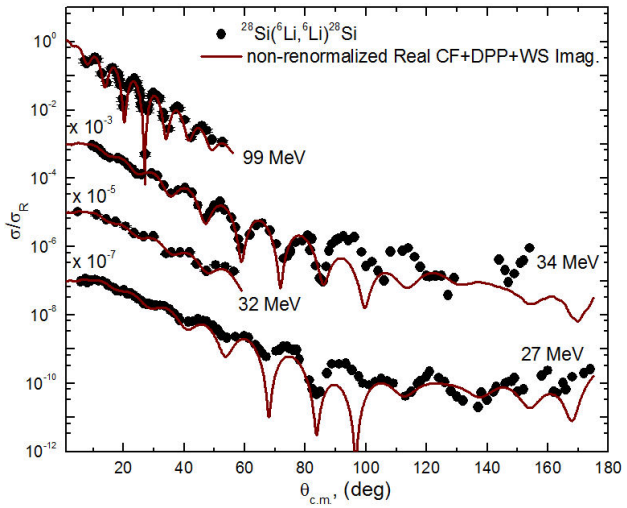

FIGURE 10. Same as Fig. 9 but at $E_{\rm lab} = 99$, 34, 32, and 27 MeV.

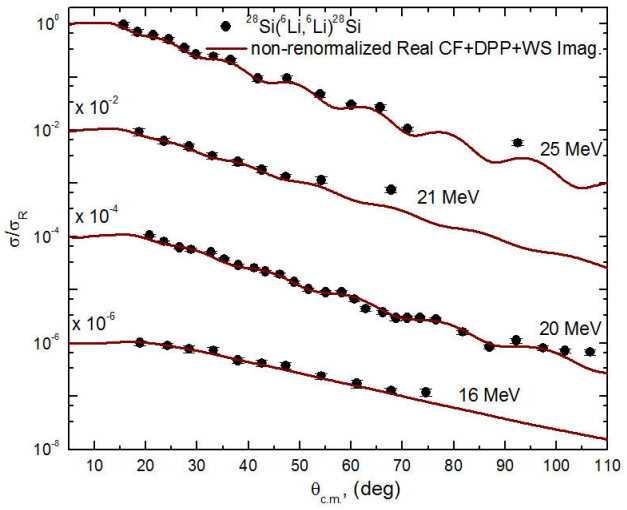

FIGURE 11. Same as Fig. 9 but at $E_{\rm lab} = 25$, 21, 20, and 16 MeV.

per interacting nucleon pair (J_R and J_i) as well as the total reaction cross sections σ_R in mb, are presented in Tables I and II, respectively. The extracted values for the total reaction cross-section σ_R as well as the real volume integral are described graphically in Fig. 12. As shown in this figure, the σ_R for CF and OM potentials has approximately the same energy behavior. After comparison, we found that the extracted values of σ_R and J_R are in good agreement with the previously reported values from Refs. [7,10,12-14,19].

4. Summary

The experimental angular distributions for ^{6}Li + ^{28}Si at $E_{lab} = 16 - 318$ MeV are reanalyzed using Woods- Saxon OM potential consisting of four varying parameters $-V_0$, a_V, W_0, and a_W depth and diffuseness for both the utilized real and imaginary volume terms while, the radii parameters $-r_V$ and r_W were kept fixed. The agreement between the experimental data and the theoretical calculations is reasonably good not only at the different concerned energies but also over the entire angular range. These data are also reanalyzed within the framework of CFOM. In this model, the real part of the potential was constructed on the basis of cluster folding, while the imaginary part was taken in the WS form as in OM analysis using the same parameters. In this case, the data are fitted with only one parameter- N_{RCF}. The obtained average value of N_{RCF} is 0.732 ± 0.1, suggesting that the strength of N_{RCF} should be reduced by about 27% in order to reproduce the data. The same problem was reported previously in DF analysis for the ^{6}Li + ^{28}Si nuclear system. Calculations performed using non-renormalized real CFP, "*i.e*, $N_{RCF} = 1$" could reproduce the data fairly by introducing a DPP surface potential term with a repulsive real part to simulate the polarization effects caused by ^{6}Li break-up. Finally, the experimental data for the ^{6}Li + ^{28}Si nuclear system, plotted as a function of momentum transfer, showed interference peaks and valleys line up and exhibit dips form at the momentum transfers around $q = 0.59$, 1.05, and 1.58 fm^{-1} that can be followed down to an energy of 34 MeV. Consequently, it should be shown that the forward angle dips are produced by the same "potential" and the differences between the cross-sections at different energies, at larger momentum transfer (angles), are due to the absorption at larger values.

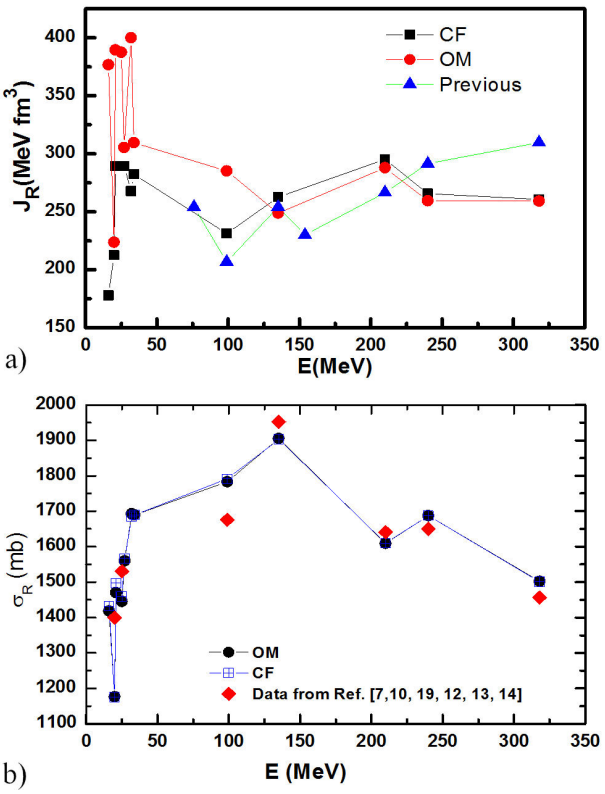

FIGURE 12. Energy dependence of the reaction cross-sections as well as real volume integral extracted from OM and CF calculations and compared with the available data from Refs. [7,10,12-14,19].

Acknowledgments

Awad A. Ibraheem extends his appreciation to the Deanship of Scientific Research at King Khalid University for funding this work through the research groups program under grant number R.G.P.1/1/42.

1. A. Pakou *et al., Phys. Lett. B* **556** (2003) 21. https://doi.org/10.1016/j.nuclphysa.2006.12.007
2. A. Pakou *et al., Phys. Rev. Lett* **90** (2003) 202701. https://doi.org/10.1103/PhysRevLett.90.202701
3. A. Pakou *et al., Phys. Rev. C* **76** (2007) 054601. https://doi.org/10.1103/PhysRevC.76.054601
4. A. Pakou *et al., Phys. Lett. B* **633** (2006) 691. https://doi.org/10.1016/j.physletb.2005.11.088
5. M. Sinha *et al., EPJ Web of Conf.* **17** (2011) 03004. https://doi.org/10.1051/epjconf/20111703004
6. K. Bethge, C. M. Fou and R. W. Zurmuhle, *Nucl. Phys. A* **123** (1969) 521. https://doi.org/10.1016/0375-9474(72)90130-3
7. M. Hugi, J. Lang, R. Muller and E. Ungricht, *Nucl. Phys. A* **368** (1981) 173. https://doi.org/10.1016/0375-9474(81)90739-9
8. M. F. Vineyard, J. Cook and K. W. Kemper, *Nucl. Phys. A* **405** (1983) 429. https://doi.org/10.1103/PhysRevC.30.916
9. N. Anantaraman, H. W. Fulbright and P. M. Stwertka, *Phys. Rev. C* **22** (1980) 501. https://doi.org/10.1103/PhysRevC.22.501
10. P. Schwandt, W. W. Jacobs, M. D. Kaitchuck and P. P. Sing, *Phys. Rev. C* **24** (1981) 1522. https://doi.org/10.1103/PhysRevC.24.1522
11. R. M. DeVries, D. A. Goldberg, J. W. Watson, M. S. Zisman and J. G. Cramer, *Phys. Rev. Lett.* **39** (1977) 450. https://doi.org/10.1103/PhysRevLett.39.450
12. A. Nadasen *et al., Phys. Rev. C* **39** (1989) 536. https://doi.org/10.1103/PhysRevC.39.536
13. X. Chen,Y. - W. Lui, H. L. Clark, Y. Tokimoto, and D. H. Youngblood, *Phys. Rev. C* **80** (2009) 014312. https://doi.org/10.1103/PhysRevC.80.014312
14. A. Nadasen *et al., Phys. Rev C* **47** (1993) 674. https://doi.org/10.1103/PhysRevC.47.674
15. A. Gómez Camacho, A. Diaz-Torres, P. R. S. Gomes, and J. Lubian, *Phys. Rev. C* **91** (2015) 014607. https://doi.org/10.1103/PhysRevC.91.014607
16. A. Gómez Camacho, A. Diaz-Torres, P. R. S. Gomes, and J. Lubian, *Phys. Rev. C* **93** (2016) 024604. https://doi.org/10.1103/PhysRevC.93.024604
17. M. Anwar, *Phys. Rev. C* **101** (2020) 064617. https://doi.org/10.1103/PhysRevC.101.064617
18. R. I. Badran and Dana Al-Masri, *Can. J. Phys.* **91** (2013) 355. https://doi.org/10.1139/cjp-2012-0466
19. M. A. Hassanain, M. Anwar, and Kassem O. Behairy, *Phys. Rev. C* **97** (2018) 044610. https://doi.org/10.1103/PhysRevC.97.044610
20. M El-Azab Farid, Awad A Ibraheem, J H Al-Zahrani, W R Al-Harbi and M A Hassanain, *J. Phys. G: Nucl. Part. Phys.* **40** (2013) 075108. https://doi.org/10.1088/0954-3899/40/7/075108
21. Yongli Xu *et al., Phys. Rev. C* **98** (2018) 024619. https://doi.org/10.1103/PhysRevC.98.024619
22. Y. Sakuragi, *Phys. Rev. C* **35** (1987) 2161. https://doi.org/10.1103/PhysRevC.35.2161
23. G. R. Satchler and W. G. Love, *Phys. Lett. B*, **76** (1978) 23. https://doi.org/10.1016/0370-1573(79)90081-4
24. D. P. Stanley, F. Petrovich, and P. Schwandt, *Phys. Rev.C* **22** (1980) 1357. https://doi.org/10.1103/PhysRevC.22.1357
25. C. W. Glover, R. I. Cutler and K. W. Kemper, *Nucl. Phys. A* **341** (1980) 137. https://doi.org/10.1016/0375-9474(80)90366-8
26. Z. Majka, H. j. Gils and H. Rebel, *Z. Phys. A* **288** (1978) 139. https://doi.org/10.1007/BF01408643
27. M . E . Branden and G. R. Satchler, *Phys. Rep.* **285** (1997) 143. https://doi.org/10.1016/S0370-1573(96)00048-8
28. Y. Sakuragi, M. Yahiro, and M. Kamimura, *Prog. Theor. Phys. Suppl.* **89** (1986) 136. https://doi.org/10.1143/PTPS.89.136
29. Y. Sakuragi, M. Ito, Y. Hirabayashi, and C . Samanta, *Prog. Theor. Phys.* **98** (1997) 521. https://doi.org/10.1143/PTP.98.521
30. I. J. Thompson, *Comput. Phys. Rep.* **7** (1988) 167. https://doi.org/10.1016/0167-7977(88)90005-6
31. F. Hinterberger, G. Mairle, U. Schmidt-Rohr, G. J. Wagner, P. Turek, *Nucl. Phys. A* **111** (1968) 265. https://doi.org/10.1016/0375-9474(68)90750-1
32. B. Tatischeff and I. Brissaud, *Nucl. Phys. A* **155** (1970) 89. https://doi.org/10.1016/0375-9474(70)90080-1
33. Sh. Hamada and Awad A. Ibraheem, *Int. J. Mod. Phys. E* **28** (2019) 1950108. https://doi.org/10.1142/S0218301319501088
34. D. A. Goldberg, S. M. Smith, G. F. Burdzik, *Phys. Rev. C* **10** (1362) 1974. https://doi.org/10.1103/PhysRevC.10.1362

35. P. Schwandt, S. Kailas, W. W. Jacobs, M. D. Kaitchuck, W. Ploughe, *Phys. Rev. C* **21** (1656) 1980. https://doi.org/10.1103/PhysRevC.21.1656

36. M. E. Brandan, *Phys. Rev. Lett*. **49** (1132) 1982. https://doi.org/10.1103/PhysRevLett.49.1132

37. M. Buenerd *et al., Phys. Rev. C* **26** (1299) 1982. https://doi.org/10.1016/0375-9474(84)90186-6